JCIM JOURNAL OF CHEMICAL INFORMATION AND MODELING

pubs.acs.org/jcim Article

Tunneling and Nonadiabatic Effects on a Proton-Coupled Electron Transfer Model for the Q_o Site in Cytochrome bc_1

Sofia R. G. Camilo,[†] Felipe Curtolo,[†] Vanesa V. Galassi, and Guilherme M. Arantes*

Cite This: *J. Chem. Inf. Model.* 2021, 61, 1840−1849 Read Online

ACCESS | Metrics & More | Article Recommendations | SI Supporting Information

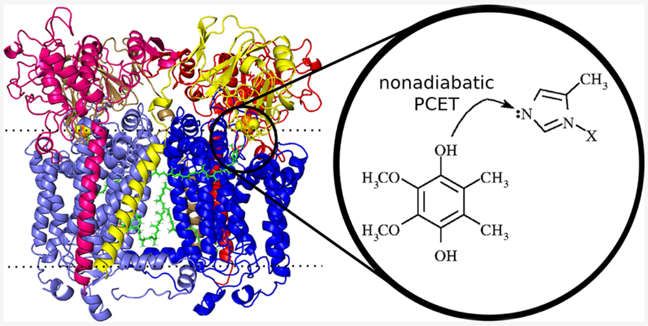

ABSTRACT: Cytochrome bc_1 is a fundamental enzyme for cellular respiration and photosynthesis. This dimeric protein complex catalyzes a proton-coupled electron transfer (PCET) from the reduced coenzyme-Q substrate (Q) to a bimetallic iron−sulfur cluster in the Q_o active site. Herein, we combine molecular dynamics simulations of the complete cytochrome bc_1 protein with electronic-structure calculations of truncated models and a semiclassical tunneling theory to investigate the electron−proton adiabaticity of the initial reaction catalyzed in the Q_o site. After sampling possible orientations between the Q substrate and a histidine side chain that functions as hydrogen acceptor, we find that a truncated model composed by ubiquinol-methyl and imidazole-iron(III)-sulfide captures the expected changes in oxidation and spin states of the electron donor and acceptor. Diabatic electronic surfaces obtained for this model with multiconfigurational wave function calculations demonstrate that this reaction is electronic nonadiabatic, and proton tunneling is faster than mixing of electronic configurations. These results indicate the formalism that should be used to calculate vibronic couplings and kinetic parameters for the initial reaction in the Q_o site of cytochrome bc_1. This framework for molecular simulation may also be applied to investigate other PCET reactions in the Q-cycle or in various metalloproteins that catalyze proton translocation coupled to redox processes.

■ INTRODUCTION

Cytochrome bc_1, also known as respiratory complex III or more precisely coenzyme-Q:cytochrome *c*-oxidoreductase, is an essential enzyme for cellular respiration and photosynthetic processes.[1−3] Together with the homologous cytochrome b_6f, these protein complexes replenish coenzyme-Q (or simply Q) levels and transfer protons across biological membranes harboring electron transfer chains by catalysis of the Q-cycle, a series of redox reactions proposed in the 1970s by Peter Mitchell.[4]

In current versions of the Q-cycle,[3,6,7] a Q substrate in quinol form binds to the Q_o site of the cytochrome bc_1 dimer[8] (Figure 1) and undergoes a bifurcated two-electron oxidation process.[9,10] One electron reduces the high-potential [2Fe-2S] cluster in the Rieske subunit, and another electron reduces the low-potential heme b_L in the *cyt b* subunit, which are reoxidized in the following steps of the Q-cycle.[11] In concert with Q oxidation, a proton bound to quinol is transferred to a histidine side chain (His152 in *Rhodobacter sphaeroids* numbering) directly bound to the [2Fe-2S] cluster.[12] This initial reaction, proposed as the rate-limiting step of the entire Q-cycle,[2,13] is a multiple-site[14] proton-coupled electron transfer (PCET) process.[15,16]

Several enzymes employ PCET as a strategy to decrease the overpotential that would have to be surmounted for electron or proton transfer alone.[16,17] Their catalytic mechanisms have been studied with molecular simulation, particularly for analysis of the tunneling behavior and participation of electronic excited states.[18−20] Although various aspects of cytochrome bc_1 have already been investigated by simulations,[21−25] proton tunneling and nonadiabatic effects of reactions in the Q_o site have received less attention.[26,27]

To advance our understanding of the Q-cycle and its associated PCET steps, it would be valuable to calculate reaction rates and isotope effects from molecular simulations of different mechanistic proposals, for steps described above in the Q_o site and for possible short-circuit reactions.[28] Comparison between calculated and measured kinetic parameters would help to validate (or exclude) a given mechanistic proposal.

The theory to calculate PCET rates has been extended by Cukier et al.[29] and Hammes-Schiffer and co-workers,[19,30] based on the treatment of nonadiabatic electron transfer[31,32] using Fermi's golden rule and linear response formalism.

Received: January 4, 2021
Published: April 1, 2021

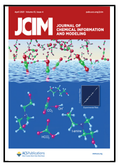

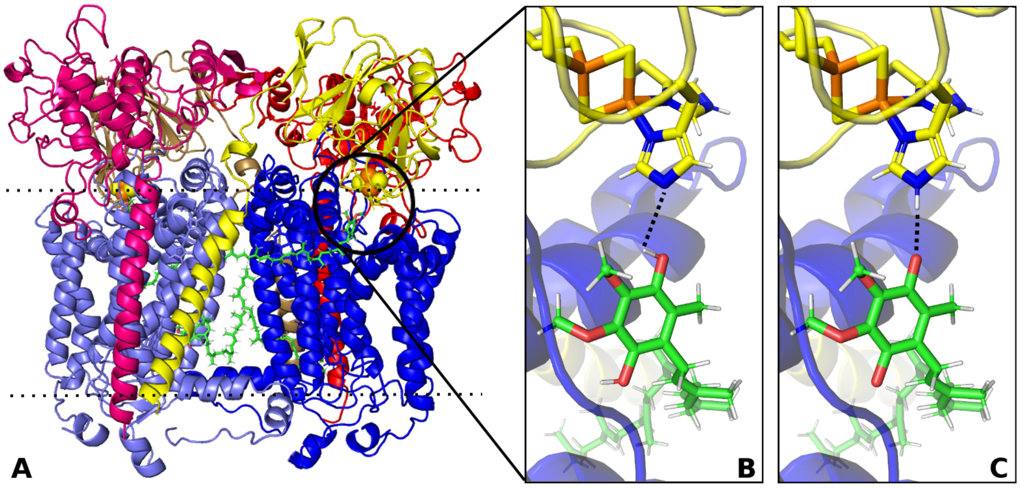

Figure 1. Structure of cytochrome bc_1 from *Rhodobacter sphaeroids* (PDB 2QJP[5]). (A) Cartoon representation with subunits cyt *b* in light and dark blue, cyt c_1 in light and dark red, and Rieske proteins in gold and yellow. Dashed black line shows the membrane boundaries. (B, C) Zoom in of one of the Q_o active sites, with ubiquinone-6 (Q) in green sticks and the [2Fe-2S] cluster with bound His and Cys side chains in yellow. A possible hydrogen bond is shown in the dashed line. Reactant state with Q in the quinol form and deprotonated His152 side chain is shown in B, and product state with Q in the quinone form and protonated His152 is shown in C.

Assuming that only one initial (donor D) and one final (acceptor A) vibronic states of the transferred proton are involved, the PCET rate may be calculated from the probability of proton tunneling at the transition state times the weighted frequency of occurrence of transition configurations as

$$k = \frac{|V_{DA}|^2}{\hbar}\sqrt{\frac{\pi}{\lambda k_B T}}\, e^{-\Delta G^{\ddagger}/k_B T} \tag{1}$$

where V_{DA} is the vibronic coupling (or tunneling matrix element[33]), λ is the environment reorganization energy, $\hbar$ is the Planck constant, k_B is the Boltzmann constant, T is the temperature, and $\Delta G^{\ddagger}$ is the activation free energy, which may be obtained from the free energy of reaction ($\Delta G°$) using relations of Marcus parabolas.[31]

The proton dynamics and the formalism used to calculate V_{DA} depend on the electronic adiabaticity, i.e., the energy separation between electronic ground and excited potential energy surfaces near transition state configurations. This key element to estimate PCET rates is explored here for a model reaction of the Q_o site employing the semiclassical treatment proposed by Georgievskii and Stuchebrukhov[33] to account for proton tunneling in between electronic adiabatic and non-adiabatic limits (see Methods for further theoretical details).

Accurate calculation of electronic surfaces for systems containing polynuclear transition-metal clusters, such as the [2Fe-2S] center in the Q_o site, is an intimidating task for quantum chemical methods. Standard multiconfigurational wave function methods suffer from an exponential explosion in the number of possible electronic configurations because of the strong correlation between many open-shell electrons in the metal centers.[34−36] Although density functional theory (DFT), particularly in the broken-symmetry approximation, has been used to study metal clusters,[37,38] it is unable to describe electronic excited and charge-transfer states. Even for single metal complexes, time-dependent DFT fails considerably.[39,40]

Herein, we seek a small truncated model of the Q_o site that may be treated with multiconfigurational electronic structure methods and still captures the essential physics of the initial PCET reaction. We explore a concerted proton−electron transfer (CPET) mechanism, since observations such as kinetic isotope effects[41] suggest this PCET reaction proceeds in one concurrent step. Classical molecular dynamics (MD) simulations of the full cytochrome bc_1 complex embedded in a membrane are used to sample relative conformations of donor (Q)−acceptor (His) groups of reactant and product states in the Q_o site. Then, density functional theory (DFT) is used to compute proton transfer profiles for various truncated models in the sampled orientations. We find that transfer from quinol to imidazole-iron(III)-sulfide is a reasonable model and use it to calculate (quasi-diabatic) localized electron transfer states with high-level (NEVPT2)[42] wave function methods. Finally, tunneling and adiabaticity parameters are determined with a semiclassical treatment, allowing us to conclude that the initial PCET in the Q_o site is vibronic nonadiabatic. As we employ truncated models for the electronic-structure calculations, our results will not be rigorously correct at the quantitative level. However, we expect the qualitative conclusions obtained here are adequate and similar to what would be obtained with more complete models for cytochrome bc_1.

■ METHODS

Molecular Dynamics of Complete Cytochrome *bc*$_1$. A complete model of the cytochrome bc_1 protein complex was built from the X-ray crystal structure of *Rhodobacter sphaeroids* (PDB 2QJP,[5] Figure 1). Inhibitors, crystallographic water, and detergent molecules were removed. Six tetra-linoleoyl cardiolipins were added according to their positions taken from a superimposed yeast model (PDB 1KB9[43]). Ubiquinone-6 (Q_6, with six isoprenoid units) was modeled in both Q_i sites of the dimer in the oxidized form with positions adjusted by manual docking in PyMOL[44] with the Q-head replacing the antimycin inhibitor and isoprenoid units in a U-shaped conformation.

Two states were described in the Q_o site, according to Figure 1B and C. In the reactant state, Q_6 was modeled in the reduced quinol (QH_2) form, and His152 was deprotonated. Also, the [2Fe-2S] center was in oxidized form. In the product state, Q_6 was modeled as an oxidized quinone, with His152 protonated (in N_ϵ, with N_δ bound to iron) and the [2Fe-2S] center reduced. Q was also placed manually with the Q-head replacing stigmatellin and isoprenoid units in an extended conformation.

Protonation states of side chains were adjusted to neutral pH (positive charge for K and R, negative for D and E, and neutral for all other residues), except for Asp373 exposed to the membrane in chains A and D, which was protonated. WhatIf[45] was used to assign His protonation and correct any missing side-chain atoms. His131 also bound to the FeS center was always protonated (in N_ϵ).

The protein complex was embedded[46] in a solvated POPC (1-palmitoyl-2-oleoyl-*sn*-glycero-3-phosphocholine) membrane with 512 lipid molecules, 39,102 water molecules, and 214 Na^+ and 158 Cl^- ions to keep the total system charge neutral and the salt concentration ≈ 0.1 M. The model has a total of 215,264 atoms. It was relaxed during four MD simulations of 50 ns each, with protein heavy atoms tethered to their initial position by harmonic restraints, successively diminished in each run, down to zero in the final one. The final production trajectory run was 540−550 ns for each state.

Interactions of protein, lipids, and ions were described with the all-atom CHARMM36 force field.[47,48] Water was represented by standard TIP3P.[49] Our calibrated force field was used for Q.[50,51] FeS centers were described using the Chang and Kim[52] parameters with corrections proposed by McCullagh and Voth.[53] Heme groups were described in oxidized form with parameters by Luthey-Schulten et al.[54] All MD simulations were performed with GROMACS version 2016.3[55] at a constant temperature of 310 K, pressure of 1 atm, and time step of 2 fs. Long-range electrostatics were treated with the particle mesh Ewald method.[56] Visualization and figure plotting were done using PyMOL[44] and Matplotlib.[57]

Electronic-Structure of Model Reactions. The PCET from ubiquinol-methyl to N-substituted methyl-imidazole (Figure 2) was studied as a model of the initial reaction of the Q-cycle in the Q_o site of cytochrome bc_1 (Figure 1). Five substituents were considered with total charge and spin as given in Table 1. The proton coordinate was defined as *PC* = d(OH) − d(NH), the transferred hydrogen distance to the donor oxygen minus the hydrogen distance to the nitrogen acceptor. Reaction paths were obtained by relaxed scans of the potential energy surface along this proton coordinate with a fixed donor−acceptor distance [d(ON)] and dihedral angle between the Q and imidazole rings to retain the protein conformation. The B3LYP DFT functional[58] and the 6-31G* basis set[59] implemented in the Gaussian 09 suite[60] were used. Partial charges and spins were obtained with Mulliken population analysis.[61]

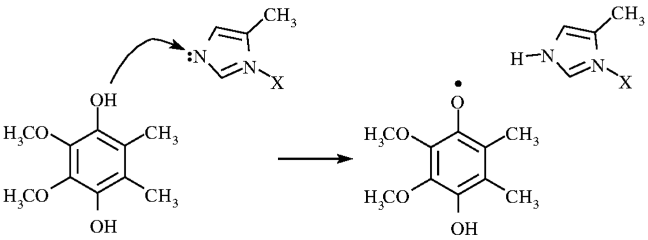

Figure 2. Model of the initial reaction in the Q_o site studied here with electronic-structure methods, X = {H, Fe^{3+}, Fe^{2+}, $[Fe\text{-}S]^{+1}$, $[Fe(SH)_3]^0$}.

Table 1. Total System Charge and Spin Multiplicity for Each Model Reaction and Given X Group of Figure 2

X	Charge	Multiplicity
H	0	1
Fe^{3+}	+2	6
Fe^{2+}	+1	5
$[Fe\text{-}S]^{+1}$	0	6
$[Fe(SH)_3]^0$	−1	6

The proton potential experienced during tunneling was obtained for three configurations of the imidazole-iron(III)-sulfide (X = $[Fe\text{-}S]^{+1}$) reaction (Tables S1−S3, Supporting Information, SI). Two configurations were taken from the constrained geometry optimizations described above at the top of the barrier near the transition state (TS) with d(ON) = 2.7 and 3.1 Å. These are called the TS orientation and show a 45° angle between planes of the Q-ring and the imidazole ring. Another configuration with the two rings coplanar and d(ON) = 2.7 Å was obtained with relaxed optimization in the B3LYP/6-31G* level and corresponds to orientations observed closer to the reactant basin. Structures along the proton coordinate were built by interpolating the proton position over the arc connecting donor and acceptor atoms, thus preserving the O−H−N angle (∼178°), with all other nuclei fixed.

Complete active space self-consistent field (CASSCF)[61] calculations were performed for these three geometry sets with the PySCF package version 1.6[62] in a sextet spin state, C_1 point-group symmetry, and def2-SVP basis set.[63] The active space contained 17 electrons in 14 molecular orbitals (MOs), CAS(17e^-, 14*o*). It is composed of seven π MOs of the ring system and conjugated H-donor oxygen in Q, five Fe 3*d* MOs, and two sulfide MOs ($3p_x$ and $3p_y$ MOs involved in metal π bonding) with 4 e^-. In the oxidized state, the π system in Q holds eight e^-, and Fe holds five e^- (13 e^- in total). In the reduced state, the π system holds seven e^-, and Fe holds six e^-. The N-electron valence state perturbation theory in second-order NEVPT2[42] was applied to the CASSCF solution to recover some dynamic electron correlation. For comparison, proton potentials were also calculated with DFT functionals B3LYP (in a vacuum and in the CPCM solvent model[64] with ϵ = 3) and ωB97X.[65]

CASSCF calculations started from the reactant (product) geometry for the oxidized (reduced) state, and guess MOs for the following geometry along the proton coordinate were taken from the previous one. The oxidized state (formally Fe^{3+}) was obtained from state-specific CASSCF with one root, and the reduced state (formally Fe^{2+}) was obtained with state-averaged CASSCF with five roots because its Fe $3d^6$ shell is almost quintuple degenerate. Aligning Fe and S atoms along the *z*-axis, $3d_{xy}$ and $3d_{x^2-y^2}$ MOs are almost degenerate. This symmetry is due to the linear N−Fe−S orientation and will be lifted for Fe in tetrahedral coordination as in the [2Fe-2S] cluster. We report only results for the lower root ($3d_{x^2-y^2}$ doubly occupied). The NEVPT2 energy was obtained specifically for this root in the reduced state. This procedure ensures that quasi-diabatic curves for oxidized and reduced states were obtained. Weights of multiconfigurational expansions were checked to remain dominated (>99.99%) by the same configurations with localized charge character along the full range of proton coordinates.

These diabatic states can be used as a basis for a two-state model of the PCET process.[66,67] The resulting symmetric 2 × 2 Hamiltonian matrix contains the oxidized $[V_{ox}(PC)]$ and reduced $[V_{red}(PC)]$ diabatic energies in the diagonal. The off-diagonal element corresponds to the electronic coupling V^{ET} between the two diabatic states and is considered independent of the proton coordinate in the Condon approximation. Assuming the diabatic states are orthogonal and diagonalizing, this 2 × 2 Hamiltonian leads to electronically adiabatic potential energy surfaces

$$U_{0/1}(PC) = \frac{1}{2}[V_{ox}(PC) + V_{red}(PC)] \mp \frac{1}{2}\sqrt{[V_{ox}(PC) - V_{red}(PC)]^2 + 4(V^{ET})^2} \tag{2}$$

for ground (U_0) and excited (U_1) states. The V^{ET} coupling was obtained by minimizing the difference between the diabatic gap $[V_{ox}(PC) - V_{red}(PC)]$ and the V^{ET} calculated as half of the energy difference between ground and excited adiabatic states over four PC geometries nearest to the diabatic crossing point. This procedure maximizes the mixture between diabatic states in the crossing region.[67,68]

Tunneling and Adiabaticity Parameters. For the initial reaction in the Q_o site, the donor or oxidized diabatic state has the transferring electron localized on Q and the FeS center oxidized, and the acceptor or reduced state has $(1 - e^-)$ oxidized Q and the FeS center reduced. As described above, diabatic states can mix to form ground and excited adiabatic states, and an avoided crossing will appear near the diabatic crossing point.

In a PCET, diabatic curves will cross at the proton coordinate PC_c with a potential energy V_c. Proton dynamics at this region will be fundamentally different in electronic adiabatic and nonadiabatic limits. In the former, electrons respond instantaneously to the proton motion but not in the latter. The semiclassical expressions derived by Georgievskii and Stuchebrukhov[33] nicely bridge both limits by means of a factor $\kappa \in [0, 1]$ with

$$\kappa = \sqrt{2\pi p}\,\frac{e^{p\ln p - p}}{\Gamma(p + 1)} \tag{3}$$

where $\Gamma(x)$ is the gamma function. The proton adiabaticity parameter p is defined as

$$p = \frac{|V^{ET}|^2}{\hbar|\Delta F|v_t} \tag{4}$$

where ΔF is the difference between the derivatives with respect to the proton coordinate of diabatic potential energy curves at PC_c, and v_t is the tunneling "velocity" calculated from

$$v_t = \sqrt{\frac{2(V_c - E)}{m}} \tag{5}$$

where m is the proton mass, and E is the tunneling energy obtained from the proton vibrational ground state energy for the donor diabatic state. One-dimensional proton vibrational wave functions and energies were calculated with the Fourier grid Hamiltonian method[69,70] and 128 grid points, and parameters V_c and ΔF were obtained from shifted diabatic proton potentials to ensure that reactant and product ground vibronic states were degenerate.[31]

Within this semiclassical treatment,[33] an effective proton tunneling time

$$\tau_p \sim \frac{V^{ET}}{|\Delta F|v_t} \tag{6}$$

and an electronic transition time

$$\tau_e \sim \frac{\hbar}{V^{ET}} \tag{7}$$

may be considered, and the adiabaticity parameter is simply

$$p = \frac{\tau_p}{\tau_e} \tag{8}$$

When $\tau_p \gg \tau_e$, the electronic states have enough time to mix, and the proton transfer occurs on the electronically adiabatic ground state. When $\tau_p \ll \tau_e$, the electronic states do not have enough time to mix during proton tunneling, and the process is electronically nonadiabatic.[66]

Similarly, in the adiabatic (ad) limit, $p \gg 1$, $\kappa = 1$ and the vibronic coupling $V_{DA}^{(ad)}$ in eq 1 may be calculated from standard quasi-classical approximations.[33,71] In the nonadiabatic (na) limit, $p \ll 1$, $\kappa = \sqrt{2\pi p}$, and the vibronic coupling

$$V_{DA,\mu\nu}^{(na)} = V^{ET}S_{\mu\nu} \tag{9}$$

where $S_{\mu\nu}$ is the Franck−Condon overlap between the proton vibrational wave functions in donor (reactant, μ) and acceptor (product, ν) diabatic states.[19,66] Intermediate regimes[33] may be accessed with $V_{DA} = \kappa V_{DA}^{(ad)}$.

RESULTS AND DISCUSSION

Donor−Acceptor Orientation in the Q_o Site of Cytochrome bc_1. The relative conformation between donor and acceptor groups in a PCET influences their electronic coupling and should be emulated when studying the truncated model systems. Thus, we begin this study by sampling the distribution of distances and orientations between Q and His152 in the Q_o site of cytochrome bc_1 with classical MD simulations of the complete protein complex. Two compositions were tested corresponding to reactant and product states of Q oxidation (Figure 1). Although a semiquinone intermediate may also be formed during the bifurcated oxidation process, this species was not simulated. Its stability is disputed,[7,72] and an empirical force field such as the one used here is less reliable to describe interactions of an open-shell molecule.

The distribution of donor−acceptor distances in Figure 3 suggests that three binding modes may be occupied by Q in the Q_o site. The proximate mode has 2.6 Å ≤ d(ON) ≤ 3.1 Å, and a hydrogen bond is formed between Q and His152, with the black line in Figure 3C showing such a long-lived contact. The second mode has d(ON) ≈ 4 Å and no direct Q···His hydrogen bonds, but short-lived water-mediated hydrogen bonds with one or two water molecules bridging Q and His152 are observed. One-molecule water bridges also form often when d(ON) ≤ 3.1 Å. In fact, there are plenty of water molecules in the Q_o site, with an average of five molecules within 5 Å of the Q-head. The third binding mode has 6 Å ≤ d(ON) ≤ 8 Å. This may be too distant for efficient electron transfer (edge-to-edge distance between Q and the FeS center

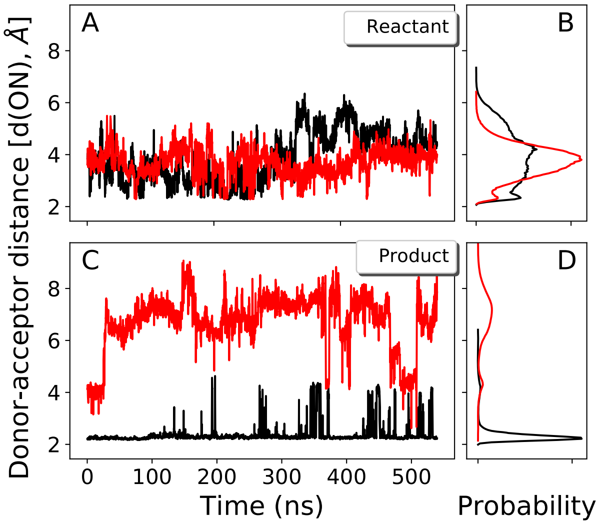

Figure 3. Molecular dynamics of Q in the Q$_o$ site of cytochrome bc_1. Trajectory (A, C) and probability distribution (B, D) of donor−acceptor distances [d(ON)] for reactant (QH$_2$···His, A and B) and product (Q···H−His, C and D) states shown in Figure 1. Results are shown for each Q$_o$ site with Rieske chain C in black and chain F in red.

≈ d(ON) + 4 Å) and probably represents an intermediate site for Q transit from or to the membrane, as found recently for another respiratory complex.[73]

For simulations with Q in the quinol form (reactant state), the proximate and third binding modes are more populated, while for simulations of the quinone form (product state) the second binding mode is mostly populated but with some occupation of the proximate mode. It is tempting to assign a mechanistic role for these occupations, but enhanced sampling and calculation of free energy profiles for binding would have to be carried out to allow for a more reliable discussion.[73,74]

In proximate and second binding modes, the relative orientation between the planes of the Q-ring and the His152 imidazole ring has a Gaussian distribution for angles ∈ [40°, 70°] with an average value of 55° independently whether the two groups are hydrogen bonded. This restriction is imposed by the active site pocket, and we have adopted a similar orientation for quantum chemical studies in the following sections. Although water-mediated transfer may play a role in PCET mechanisms,[17,75] we have not explored this possibility in the remainder of this work.

Truncated Model System for PCET from Quinol. Isolated reactions shown in Figure 2 are explored in this section as possible models of the initial PCET in the Q$_o$ site. Our goal is to find a truncated system that captures the PCET mechanism and is amenable to calculations with standard multiconfigurational electronic-structure methods, so that the many-electron quantum wave function and related non-adiabatic effects may be appreciated.

For the simplest truncated model with X = H, the results of DFT calculations in Figure S1 indicate that reaction energies and barriers for proton transfer increase monotonically with donor−acceptor distances d(ON) ∈ [2.7,4.0] Å. This is the range of d(ON) in which direct and water-mediated hydrogen bonds between Q and His152 in the Q$_o$ site were observed in the previous section. The reverse reaction is activated only in d(ON) ≥ 3.0 Å, when the forward barrier is higher than 30 kcal/mol. Both the reaction energy and barrier would decrease in a polar environment due to stabilization of the charge-separated products. However, this model with X = H cannot account for electron transfer because of the low electron affinity of imidazole, and the reaction is a pure proton transfer.

The donor−acceptor distance was fixed at d(ON) = 3.1 Å for the other model systems tested in this section. At this distance, a hydrogen bond is often found in the Q$_o$ site of the full cytochrome bc_1, and proton transfer should be an activated process, forming a stable product.

Results for the reaction with substitution X = Fe^{3+} are shown in Figure 4, with a lower barrier and a stable product for proton transfer. Population analysis shows the partial charge in the Q group increases and correspondingly decreases in the Fe center along the reaction progress, suggesting electron transfer is coupled to proton transfer (Figure 4B and Table 2). However, partial spin densities for the quinol reactant clearly demonstrate it has an unpaired electron in the reactant and, together with partial charges in Q and the transferred H, indicate an already oxidized QH$_2^{(\bullet)+}$ reactant and a two-electron oxidized product. The Fe center has four unpaired electrons in the reactant and five in the product. These are not the expected oxidation and spin states, hence not a good model, for the initial PCET reaction in the Q$_o$ site.

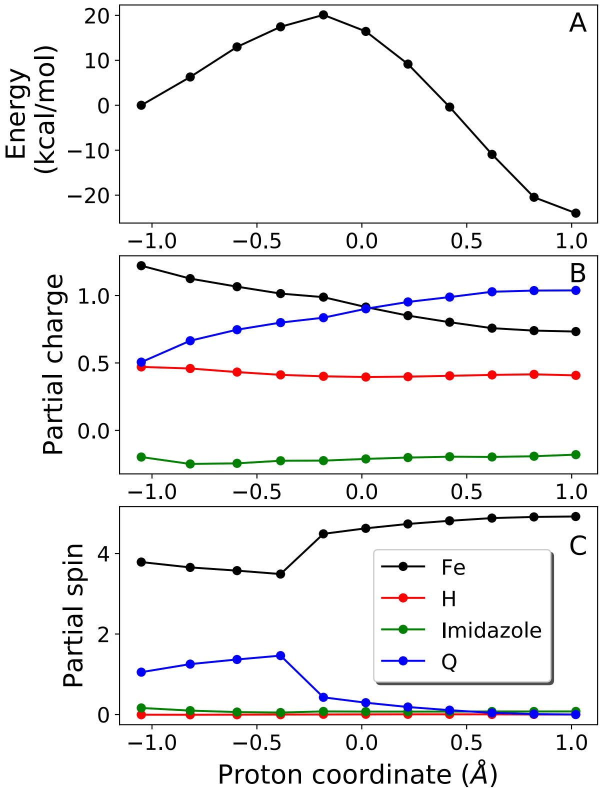

Figure 4. PCET from quinol to imidazole-iron(III), X = Fe^{3+} in Figure 2, with donor−acceptor distance d(ON) = 3.1 Å. Potential energy (A), partial charges (B), and partial spins (C) obtained at the B3LYP/6-31G* level along the proton coordinate (*PC*) for groups shown in the legend, with Q denoting quinol except for transferred H.

Note that the pitfalls of using population analysis to examine reaction mechanisms recently discussed in the context of PCET[20,76] are partially mitigated when summing populations over whole chemical groups,[77] such as in Q or imidazole groups used here.

Table 2. Partial Charges and Spins Condensed to Q (Quinol except Transferred Hydrogen) and X Groups Obtained at the B3LYP/6-31G* Level for Reactant (R, $PC = -1.0$ Å) and Product (P, $PC = 1.0$ Å) States of Model Reactions in Figure 2

	Charge				Spin			
	Q		X		Q		X	
X	R	P	R	P	R	P	R	P
Fe^{3+}	0.5	1.0	1.2	0.7	1.0	0.0	3.8	4.9
Fe^{2+}	0.4	0.1	0.6	0.7	−1.0	−1.0	4.9	4.9
$[Fe\text{-}S]^{+1}$	−0.4	0.0	0.4	0.0	0.1	0.8	4.9	4.2
$[Fe(SH)_3]^0$	−0.5	−0.7	−0.4	−0.4	0.0	0.2	4.9	4.7

Table 2 shows population analysis for reactant and product geometries of proton transfer. These properties are sufficient to check whether a PCET reaction is observed and involves the expected oxidation and spin states. The transferred H has a partial charge $q_H \in [0.4, 0.5]$ and spin $S = 0$, and the imidazole group has spin $S \approx 0$, for all X and proton coordinates (for example, see Figure 4). For substitutions X = Fe^{2+} and X = $[Fe(SH)_3]^0$, partial charges and spins on Q and on the iron center do not change significantly from reactant to product, indicating that electron transfer is not observed in concert with the proton transfer.

On the other hand, substitution X = $[Fe\text{-}S]^{+1}$ has all expected features of the initial PCET in the Q_o site. Partial charge (plus q_H of the transferred H) and spin on Q are close to zero in the reactant, whereas the Q charge remains zero, and spin is 0.8 in the product, in line with a neutral QH_2 reactant and the expected semiquinone $QH^{(\bullet)}$ radical product. For the iron center ([Fe-S]), the partial charge is reduced by the same amount increased in Q, and the number of unpaired electrons changes from 4.9 to 4.2, in line with a coupled electron transfer and reduction of the iron center from a formal Fe^{3+} d^5 to a Fe^{2+} d^6 configuration. Thus, the reaction between ubiquinol-methyl and imidazole-iron(III)-sulfide (X = $[Fe\text{-}S]^{+1}$) captures the essential PCET mechanism and is a reasonable truncated model system.

Electronic Surfaces and Couplings Indicate a Non-adiabatic PCET. The concerted PCET reaction from quinol to imidazole-iron(III)-sulfide (X = $[Fe\text{-}S]^{+1}$ in Figure 2) is investigated in this section with multiconfigurational electronic-structure theory at the NEVPT2 level. Electronic surfaces along the proton coordinate with other nuclei fixed, or proton potentials, were calculated in three donor−acceptor configurations: planar orientation with d(ON) = 2.7 Å and TS orientation with d(ON) = (2.7, 3.1) Å. The latter was obtained from constrained geometry optimizations for this truncated model and corresponds to configurations observed for direct hydrogen bonding between Q and the His152 side chain in the proximal binding mode of the Q_o site during MD simulations described above.

Figure 5 shows the surfaces for diabatic electron donor and acceptor states and the corresponding adiabatic curves. The lower energy product (red triangles in $PC > 0.5$ Å, in Figure 5) corresponds to the semiquinone $QH^{(\bullet)}$ radical and reduced iron center, as found for the DFT calculations.

The diabatic crossing point and the corresponding adiabatic avoided-crossing region are observed at $PC_c \in [0.2, 0.4]$ Å with the proton closer to the acceptor in all orientations. This confirms that proton and electron transfer are concerted, as indicated by population analysis in the previous section.

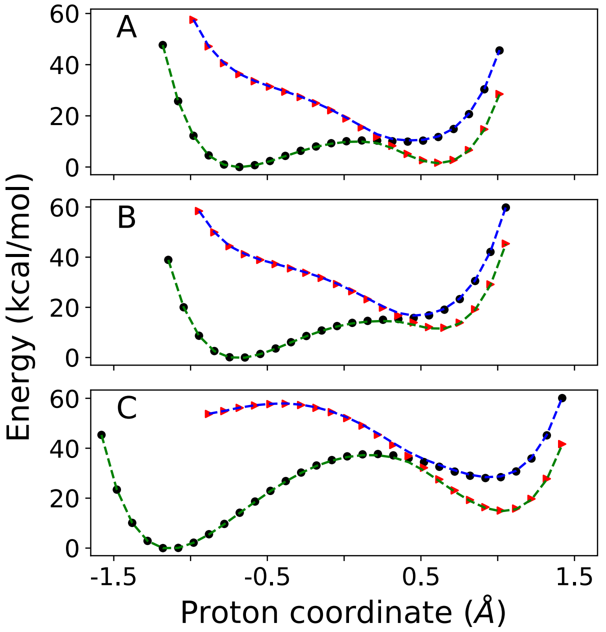

Figure 5. Proton potentials for PCET from quinol to imidazole-iron(III)-sulfide, X = $[Fe\text{-}S]^{+1}$ in Figure 2, for three donor−acceptor configurations: distance d(ON) = 2.7 Å with the Q-ring and imidazole ring coplanar (A), with rings bent in TS orientation (B), and distance d(ON) = 3.1 Å with rings bent in TS orientation (C). NEVPT2/def2-SVP potential energy was obtained along the proton coordinate for oxidized (electron localized in the Q donor, black circle) and reduced (electron localized in the iron acceptor, red triangle) diabatic states. Dashed lines represent adiabatic ground (green) and excited (blue) state surfaces obtained with eq 2.

Interestingly, this may also characterize a late multiple-site PCET[14] and suggests that catalysis by the enzymatic environment may be attained through stabilization of the reduced (acceptor) state.

Although the shapes of proton potentials are similar for the three configurations, the adiabatic reaction energy and barrier (and even the diabatic crossing energy V_c obtained after shifting the potentials, Table 3) are clearly lower for the planar orientation (Figure 5A). However, this configuration was not observed in the Q_o active site where the angle between the Q-head and the imidazole ring ∈ [40°, 70°] (see above), suggesting that any kinetic advantage from this orientation could not exhort enough evolutionary pressure to alter the stereochemistry in the Q_o site.

On a methodological note, the surfaces in Figure 5 include both static and dynamic electron correlations.[35,61] Although the latter may require larger basis sets to reach convergence, we consider the NEVPT2 electronic surfaces shown here appropriate for this initial investigation and in line with (or even more rigorous than) previous studies on adiabaticity parameters of PCET involving metal centers.[27,78]

The semiclassical treatment of Georgievskii and Stuchebrukhov,[33] eqs 3−7, was employed together with the NEVPT2 electronic surfaces to characterize the electron−proton adiabaticity of the model PCET reaction. Calculated parameters for three donor−acceptor configurations shown in Table 3 indicate significant electronic nonadiabaticity for the model PCET, as $p \ll 1$ for all configurations. Accordingly, $\tau_p \ll \tau_e$ suggests that electrons will not have enough time to rearrange and mix their electronic configurations, so the proton will tunnel between the diabatic states.

Table 3. Tunneling and Adiabaticity Parameters Defined in Eqs 3−9 and Calculated for the Imidazole-Iron(III)-Sulfide System (X = [Fe-S]$^{+1}$) in Three Donor−Acceptor Configurations[a]

	d(ON)		
	2.7 Å		3.1 Å
Orientation:	Planar	TS	TS
V^{ET} (cm^{-1})	540	560	700
V_c (kcal mol^{-1})	10.3	14.0	36.8
ΔF (kcal mol^{-1} Å^{-1})	34.9	40.5	38.7
E (kcal mol^{-1})	1.95	2.12	2.45
v_t (× 10^3 m/s)	8.28	9.92	16.9
p	0.055	0.042	0.040
κ	0.488	0.441	0.434
τ_p (fs)	0.537	0.399	0.306
τ_e (fs)	9.79	9.49	7.59
S_{00} (× 10^{-6})	19.8	6.14	0.642
$V_{DA,00}^{(na)}$ (× 10−3 cm^{-1})	10.7	3.44	0.450

[a] S_{00} is the overlap between ground vibrational wave functions for the transferred proton in donor (μ = 0) and acceptor (ν = 0) diabatic potentials, and $V_{DA,00}^{(na)}$ is the respective nonadiabatic vibronic coupling.

For the three geometries studied, we note likewise V^{ET} values which support usage of the Condon approximation. Although the crossing energies V_c are quite different, its square-root dependence in eq 5 and the similarity of other parameters (V^{ET}, E, ΔF) result in quite close adiabaticity p and κ and effective tunneling times for the three configurations. This behavior for the truncated Q_o site model contrasts to other systems undergoing PCET for which changes in relative orientation of donor−acceptor groups result in very different V^{ET} coupling and even modification of the adiabaticity regime.[79]

Vibrational Analysis and Comparison to Previous Results. In the nonadiabatic limit, the vibronic coupling V_{DA} in eq 1 should be obtained accordingly to eq 9. Thus, we calculated proton vibrational wave functions for the truncated Q_o site model using the shifted diabatic potentials in Figure 5 so that donor and acceptor ground vibronic states became degenerate, as required in the Marcus theory for electron transfer.[31] Although the calculated overlap $S_{\mu\nu}$ between excited vibrational wave functions ($\mu > 0$) is considerable, the population of donor excited vibronic states and hence their contribution to the overall vibrational coupling is low. We show in Table 3 only the overlap and V_{DA} corresponding to vibronic transitions between ground states ($\mu = \nu = 0$).

The overlap decreases 3-fold between planar and TS orientations for the same donor−acceptor separation [d(ON) = 2.7 Å], resulting in a higher vibronic coupling for the planar configuration (Table 3). Again, the planar orientation was not observed during MD simulations of the Q_o active site and should not play a role for the PCET in cytochrome bc_1. For the TS orientation, increasing the d(ON) separation by 0.4 Å resulted in a 10-fold decrease of the vibrational overlap, as expected from its exponential dependence on distance.[19] It is also noted that energies of vibrational ground states in the donor diabatic state are similar for the three orientations (within 0.5 kcal/mol, E in Table 3).

While our article was under review, another similar study of the concerted PCET reaction in the Q_o site of cytochrome bc_1 was published.[27] Barragan et al. employed a larger Q_o site model, including the complete [2Fe-2S] cluster with ligands, Q-head substrate, and some side chains to emulate the active site environment (total of 167 atoms). Due to the enlarged size, a more approximate method, constrained DFT in the configurational interaction extension (CI-CDFT),[67] was applied to obtain electronic couplings and diabatic surfaces. Barragan et al. employed the same semiclassical formalism used here[33] and also found that the PCET is vibronic nonadiabatic but with a 10-fold lower adiabaticity parameter $p = 0.004$. They obtained a higher $V^{ET} = 2000$ cm^{-1} but a lower $V_{DA,00}^{(na)} = 1.6 \times 10^{-3}$ cm^{-1} likely due to a slightly longer donor−acceptor distance [d(ON) = 2.83 Å in their model] and smaller vibrational overlap. They calculate kinetic isotope effects in good agreement with a biomimetic system[80] but 10-fold higher than those measured for reaction in the Q_o site[41] of the homologous cytochrome b_6f.

The major difference between the work of Barragan et al.[27] and our study is the composition of the Q_o site model, whereas our truncated model is much simpler particularly lacking the second iron center (and the corresponding spin-coupling[34]) and iron ligands (other sulfide and imidazole groups) found in the complete Rieske [2Fe-2S] cluster. Another important difference concerns the method used for electronic-structure calculations. Figure S2 shows that the proton potentials obtained for our truncated model with DFT functionals B3LYP and ωB97X (as used by Barragan et al.) are significantly different from the NEVPT2 curve, particularly in the reactant basin dominated by the donor diabatic state. This state is destabilized by 30−40 kcal/mol in DFT treatments probably due to the self-interaction error.[81,82] Although constrained DFT may mitigate this error,[67] Barragan et al. also observe a wide variation of electronic couplings calculated along their proton potential, suggesting the participation of multiple electronic configurations.[27] Thus, it remains to be seen whether a multiconfigurational wave function treatment of a more complete model including the bimetallic [2Fe-2S] cluster will lead to more accurate vibronic couplings and, ultimately, better agreement with experimental kinetics.

■ CONCLUSIONS

We have proposed a molecular simulation framework to analyze tunneling and electron−proton adiabaticity in PCET reactions catalyzed by metalloenzymes. The procedure combines classical MD simulations of the complete protein to sample conformations of reactive groups in the active site and electronic-structure calculations of truncated models containing donor and acceptor groups for the transferred electron and proton. The latter calculations may be conducted with DFT to efficiently screen the proposed truncated systems for models that retain the expected oxidation and spin states of donor and acceptor groups. However, multiconfigurational wave function calculations should be applied to obtain qualitatively correct diabatic surfaces when transition metals are involved in the electron transfer. The semiclassical theory for proton tunneling proposed by Georgievskii and Stuchebrukhov[33] can be used to determine the adiabaticity and the relative time scales of proton and electron transitions from the diabatic proton potentials. For a nonadiabatic transfer, vibronic couplings may be calculated from electronic coupling and vibrational analysis of the diabatic surfaces. We expect that this procedure may be applied to investigate other metalloenzymes involved in redox-coupled proton translocation.

For cytochrome bc_1, we find that the quinol substrate and quinone product in the Q_o site form direct and water-mediated hydrogen bonds with His152, and the relative orientation between Q-head and His152 imidazole rings is quite restricted. A truncated model containing ubiquinol-methyl and imidazole-iron(III)-sulfide emulates the concerted PCET mechanism and was used to obtain diabatic surfaces for electron transfer at the NEVPT2 level. In the three configurations studied, the diabatic crossing energy changes considerably, but other calculated parameters are rather similar, particularly the electronic coupling V^{ET}. Thus, the truncated Q_o site model has stable electronic and tunneling properties and can be studied to understand details of the catalytic mechanism in cytochrome bc_1. Although the calculated V^{ET} couplings are high, their product with low vibrational overlaps results in vibronic couplings much smaller than the thermal energy (k_BT) for all configurations, so tunneling in this PCET model is vibronic nonadiabatic. Kinetic parameters should be calculated with theory appropriate for this limit.

The proposed framework and the results obtained for cytochrome bc_1 could be extended in several ways. To increase model realism, the complete protein and the environment solvating reactive groups could be investigated with hybrid QM/MM potentials.[83−85] The electronic structure of excited and charge-transfer states for the bimetallic iron−sulfur cluster in cytochrome bc_1 or polynuclear metal centers[34] in other proteins would have to be described with advanced multiconfigurational methods, such as DMRG.[36] Rate constants and kinetic parameters could be calculated from proton potentials obtained with these more realistic models and rigorous electronic-structure treatments for further comparison with experiments.[7,27,41,72] Future work in these lines will certainly contribute to sharpen our understanding of the Q-cycle and of PCET reactions in metalloenzymes.

■ ASSOCIATED CONTENT

Supporting Information

The Supporting Information is available free of charge at https://pubs.acs.org/doi/10.1021/acs.jcim.1c00008.

> Reaction energy and barrier for the pure proton transfer reaction from quinol to imidazole, comparison of adiabatic proton potentials for PCET from quinol to imidazole-iron(III)-sulfide, and Cartesian coordinates for the three orientations used for calculation of proton potentials (PDF)

■ AUTHOR INFORMATION

Corresponding Author

Guilherme M. Arantes − *Department of Biochemistry, Instituto de Química, Universidade de São Paulo, 05508-900 São Paulo, SP, Brazil;* orcid.org/0000-0001-5356-7703; Email: garantes@iq.usp.br

Authors

Sofia R. G. Camilo − *Department of Biochemistry, Instituto de Química, Universidade de São Paulo, 05508-900 São Paulo, SP, Brazil*

Felipe Curtolo − *Department of Biochemistry, Instituto de Química, Universidade de São Paulo, 05508-900 São Paulo, SP, Brazil;* orcid.org/0000-0002-4459-0968

Vanesa V. Galassi − *Department of Biochemistry, Instituto de Química, Universidade de São Paulo, 05508-900 São Paulo, SP, Brazil*

Complete contact information is available at: https://pubs.acs.org/10.1021/acs.jcim.1c00008

Author Contributions

[†]S. R. G. Camilo and F. Curtolo have contributed equally to this work and share first authorship.

Notes

The authors declare no competing financial interest.

■ ACKNOWLEDGMENTS

Funding from Fundação de Amparo à Pesquisa do Estado de São Paulo (FAPESP, Scholarship Grants 2019/05531-0 to S.R.G.C, 2017/26109-0 to F.C., and 2012/17833-2 to V.V.G., and Research Grant 2019/21856-7 to G.M.A.) and computational resources from the SDumont cluster in the National Laboratory for Scientific Computing (LNCC/MCTI) are gratefully acknowledged.

■ REFERENCES

(1) Crofts, A. R. The Cytochrome bc_1 Complex: Function in the Context of Structure. *Annu. Rev. Physiol.* **2004**, *66*, 689−733.

(2) Cramer, W.; Hasan, S. S.; Yamashita, E. The Q Cycle of Cytochrome bc Complexes: A Structure Perspective. *Biochim. Biophys. Acta, Bioenerg.* **2011**, *1807*, 788−802.

(3) Sarewicz, M.; Pintscher, S.; Pietras, R.; Borek, A.; Bujnowicz, Ł.; Hanke, G.; Cramer, W. A.; Finazzi, G.; Osyczka, A. Catalytic Reactions and Energy Conservation in the Cytochrome bc1 and b6f Complexes of Energy-Transducing Membranes. *Chem. Rev.* **2021**, *121*, 2020−2108.

(4) Mitchell, P. The Protonmotive Q-cycle: A General Formulation. *FEBS Lett.* **1975**, *59*, 137−139.

(5) Esser, L.; Elberry, M.; Zhou, F.; Yu, C.-A.; Yu, L.; Xia, D. Inhibitor-Complexed Structures of the Cytochrome bc_1 from the Photosynthetic Bacterium *Rhodobacter sphaeroides*. *J. Biol. Chem.* **2008**, *283*, 2846−2857.

(6) Osyczka, A.; Moser, C. C.; Dutton, P. L. Fixing the Q-Cycle. *Trends Biochem. Sci.* **2005**, *30*, 176−182.

(7) Crofts, A. R.; Holland, J. T.; Victoria, D.; Kolling, D. R.; Dikanov, S. A.; Gilbreth, R.; Lhee, S.; Kuras, R.; Kuras, M. G. The Q-cycle Reviewed: How Well Does a Monomeric Mechanism of the bc_1 Complex Account for the Function of a Dimeric Complex? *Biochim. Biophys. Acta, Bioenerg.* **2008**, *1777*, 1001−1019.

(8) Xia, D.; Esser, L.; Tang, W.-K.; Zhou, F.; Zhou, Y.; Yu, L.; Yu, C.-A. Structural Analysis of Cytochrome bc_1 Complexes: Implications to the Mechanism of Function. *Biochim. Biophys. Acta, Bioenerg.* **2013**, *1827*, 1278−1294.

(9) Nitschke, W.; Russell, M. J. Redox Bifurcations: Mechanisms and Importance to Life Now, and at Its Origin. *BioEssays* **2012**, *34*, 106−109.

(10) Yuly, J. L.; Zhang, P.; Lubner, C. E.; Peters, J. W.; Beratan, D. N. Universal Free-Energy Landscape Produces Efficient and Reversible Electron Bifurcation. *Proc. Natl. Acad. Sci. U. S. A.* **2020**, *117*, 21045−21051.

(11) Havens, J.; Castellani, M.; Kleinschroth, T.; Ludwig, B.; Durham, B.; Millett, F. Photoinitiated Electron Transfer within the *Paracoccus denitrificans* Cytochrome bc_1 Complex: Mobility of the Iron-Sulfur Protein Is Modulated by the Occupant of the Q_o Site. *Biochemistry* **2011**, *50*, 10462−10472.

(12) Hsueh, K.-L.; Westler, W. M.; Markley, J. L. NMR Investigations of the Rieske Protein from *Thermus thermophilus* Support a Coupled Proton and Electron Transfer Mechanism. *J. Am. Chem. Soc.* **2010**, *132*, 7908−7918.

(13) Crofts, A. R.; Guergova-Kuras, M.; Kuras, R.; Ugulava, N.; Li, J.; Hong, S. Proton-coupled Electron Transfer at the Q_o Site: What Type of Mechanism Can Account for the High Activation Barrier? *Biochim. Biophys. Acta, Bioenerg.* **2000**, *1459*, 456−466.

(14) Darcy, J. W.; Koronkiewicz, B.; Parada, G. A.; Mayer, J. M. A Continuum of Proton-Coupled Electron Transfer Reactivity. *Acc. Chem. Res.* **2018**, *51*, 2391−2399.

(15) Zu, Y.; Couture, M. M.-J.; Kolling, D. R. J.; Crofts, A. R.; Eltis, L. D.; Fee, J. A.; Hirst, J. Reduction Potentials of Rieske Clusters: Importance of the Coupling between Oxidation State and Histidine Protonation State†. *Biochemistry* **2003**, *42*, 12400−12408.

(16) Huynh, M. H. V.; Meyer, T. J. Proton-Coupled Electron Transfer. *Chem. Rev.* **2007**, *107*, 5004−5064.

(17) Dempsey, J. L.; Winkler, J. R.; Gray, H. B. Proton-Coupled Electron Flow in Protein Redox Machines. *Chem. Rev.* **2010**, *110*, 7024−7039.

(18) Poulsen, T. D.; Garcia-Viloca, M.; Gao, J.; Truhlar, D. G. Free Energy Surface, Reaction Paths, and Kinetic Isotope Effect of Short-Chain Acyl-CoA Dehydrogenase. *J. Phys. Chem. B* **2003**, *107*, 9567−9578.

(19) Hammes-Schiffer, S.; Stuchebrukhov, A. A. Theory of Coupled Electron and Proton Transfer Reactions. *Chem. Rev.* **2010**, *110*, 6939−6960.

(20) Curtolo, F.; Arantes, G. M. Mechanisms for Flavin-Mediated Oxidation: Hydride or Hydrogen-Atom Transfer? *J. Chem. Inf. Model.* **2020**, *60*, 6282.

(21) Crofts, A. R.; Hong, S.; Wilson, C.; Burton, R.; Victoria, D.; Harrison, C.; Schulten, K. The mechanism of ubihydroquinone oxidation at the Q_o-site of the cytochrome bc_1 complex. *Biochim. Biophys. Acta, Bioenerg.* **2013**, *1827*, 1362−1377.

(22) Martin, D. R.; Matyushov, D. V. Microsecond Dynamics of the Protein and Water Affect Electron Transfer in a Bacterial bc_1 Complex. *J. Chem. Phys.* **2015**, *142*, 161101.

(23) Hagras, M. A.; Stuchebrukhov, A. A. Internal Switches Modulating Electron Tunneling Currents in Respiratory Complex III. *Biochim. Biophys. Acta, Bioenerg.* **2016**, *1857*, 749−758.

(24) Postila, P. A.; Kaszuba, K.; Kuleta, P.; Vattulainen, I.; Sarewicz, M.; Osyczka, A.; Róg, T. Atomistic Determinants of co-Enzyme Q Reduction at the Q_i-Site of the Cytochrome bc_1 Complex. *Sci. Rep.* **2016**, *6*, 33607.

(25) Barragan, A. M.; Schulten, K.; Solov'yov, I. A. Mechanism of the Primary Charge Transfer Reaction in the Cytochrome bc1 Complex. *J. Phys. Chem. B* **2016**, *120*, 11369−11380.

(26) Ludlow, M. K.; Soudackov, A. V.; Hammes-Schiffer, S. Theoretical Analysis of the Unusual Temperature Dependence of the Kinetic Isotope Effect in Quinol Oxidation. *J. Am. Chem. Soc.* **2009**, *131*, 7094−7102.

(27) Barragan, A. M.; Soudackov, A. V.; Luthey-Schulten, Z.; Hammes-Schiffer, S.; Schulten, K.; Solov'yov, I. A. Theoretical Description of the Primary Proton-Coupled Electron Transfer Reaction in the Cytochrome bc1 Complex. *J. Am. Chem. Soc.* **2021**, *143*, 715−723.

(28) Springett, R. The Proton Pumping Mechanism of the bc Complex. *Biochim. Biophys. Acta, Bioenerg.* **2021**, *1862*, 148352.

(29) Cukier, R. I.; Nocera, D. G. Proton-Coupled Electron Transfer. *Annu. Rev. Phys. Chem.* **1998**, *49*, 337−369.

(30) Soudackov, A.; Hammes-Schiffer, S. Derivation of Rate Expressions for Nonadiabatic Proton-Coupled Electron Transfer Reactions in Solution. *J. Chem. Phys.* **2000**, *113*, 2385−2396.

(31) Marcus, R. A.; Sutin, N. Electron Transfers in Chemistry and Biology. *Biochim. Biophys. Acta, Rev. Bioenerg.* **1985**, *811*, 265−322.

(32) Blumberger, J. Recent Advances in the Theory and Molecular Simulation of Biological Electron Transfer Reactions. *Chem. Rev.* **2015**, *115*, 11191−11238.

(33) Georgievskii, Y.; Stuchebrukhov, A. A. Concerted Electron and Proton Transfer: Transition from Nonadiabatic to Adiabatic Proton Tunneling. *J. Chem. Phys.* **2000**, *113*, 10438−10450.

(34) Arantes, G. M.; Taylor, P. R. Approximate Multiconfigurational Treatment of Spin-Coupled Metal Complexes. *J. Chem. Theory Comput.* **2010**, *6*, 1981−1989.

(35) Arantes, G. M.; Bhattacharjee, A.; Field, M. J. Homolytic Cleavage of Fe−S Bonds in Rubredoxin Under Mechanical Stress. *Angew. Chem., Int. Ed.* **2013**, *52*, 8144−8146.

(36) Sharma, S.; Sivalingam, K.; Neese, F.; Chan, G. K.-L. Low-Energy Spectrum of Iron-Sulfur Clusters Directly from Many-Particle Quantum Mechanics. *Nat. Chem.* **2014**, *6*, 927−933.

(37) Noodleman, L.; Peng, C.; Case, D.; Mouesca, J.-M. Orbital Interactions, Electron Delocalization and Spin Coupling in Iron-Sulfur Clusters. *Coord. Chem. Rev.* **1995**, *144*, 199−244.

(38) Noodleman, L.; Han, W.-G. Structure, Redox, pKa, Spin. A Golden Tetrad for Understanding Metalloenzyme Energetics and Reaction Pathways. *JBIC, J. Biol. Inorg. Chem.* **2006**, *11*, 674−694.

(39) Neese, F. A. Critical Evaluation of DFT, Including Time-Dependent DFT, Applied to Bioinorganic Chemistry. *JBIC, J. Biol. Inorg. Chem.* **2006**, *11*, 702−711.

(40) Arantes, G. M.; Field, M. J. Ferric-Thiolate Bond Dissociation Studied with Electronic Structure Calculations. *J. Phys. Chem. A* **2015**, *119*, 10084−10090.

(41) Soriano, G. M.; Cramer, W. A. Deuterium Kinetic Isotope Effects in the p-Side Pathway for Quinol Oxidation by the Cytochrome b6f Complex. *Biochemistry* **2001**, *40*, 15109−15116.

(42) Angeli, C.; Cimiraglia, R.; Evangelisti, S.; Leininger, T.; Malrieu, J.-P. Introduction of n-Electron Valence States for Multi-reference Perturbation Theory. *J. Chem. Phys.* **2001**, *114*, 10252−10264.

(43) Lange, C.; Nett, J. H.; Trumpower, B. L.; Hunte, C. Specific Roles of Protein-Phospholipid Interactions in the Yeast Cytochrome bc_1 Complex Structure. *EMBO J.* **2001**, *20*, 6591−6600.

(44) *PyMOL Molecular Graphics System*, Version 1.8; Schrödinger, LLC, 2015.

(45) Vriend, G. WHAT IF: a Molecular Modeling and Drug Design Program. *J. Mol. Graphics* **1990**, *8*, 52−56.

(46) Javanainen, M. Universal Method for Embedding Proteins into Complex Lipid Bilayers for Molecular Dynamics Simulations. *J. Chem. Theory Comput.* **2014**, *10*, 2577−2582.

(47) Klauda, J. B.; Venable, R. M.; Freites, J. A.; O'Connor, J. W.; Tobias, D. J.; Mondragon-Ramirez, C.; Vorobyov, I.; MacKerell, A. D.; Pastor, R. W. Update of the CHARMM All-Atom Additive Force Field for Lipids: Validation on Six Lipid Types. *J. Phys. Chem. B* **2010**, *114*, 7830−7843.

(48) Huang, J.; MacKerell, A. D., Jr CHARMM36 All-Atom Additive Protein Force Field: Validation Based on Comparison to NMR Data. *J. Comput. Chem.* **2013**, *34*, 2135−2145.

(49) Jorgensen, W. L.; Chandrasekhar, J.; Madura, J. D.; Impey, R. W.; Klein, M. L. Comparison of Simple Potential Functions for Simulating Liquid Water. *J. Chem. Phys.* **1983**, *79*, 926−935.

(50) Galassi, V. V.; Arantes, G. M. Partition, Orientation and Mobility of Ubiquinones in a Lipid Bilayer. *Biochim. Biophys. Acta, Bioenerg.* **2015**, *1847*, 1560−1573.

(51) Teixeira, M. H.; Arantes, G. M. Effects of Lipid Composition on Membrane Distribution and Permeability of Natural Quinones. *RSC Adv.* **2019**, *9*, 16892−16899.

(52) Chang, C. H.; Kim, K. Density Functional Theory Calculation of Bonding and Charge Parameters for Molecular Dynamics Studies on [FeFe] Hydrogenases. *J. Chem. Theory Comput.* **2009**, *5*, 1137−1145.

(53) McCullagh, M.; Voth, G. A. Unraveling the Role of the Protein Environment for [FeFe]-Hydrogenase: A New Application of Coarse-graining. *J. Phys. Chem. B* **2013**, *117*, 4062−4071.

(54) Autenrieth, F.; Tajkhorshid, E.; Baudry, J.; Luthey-Schulten, Z. Classical force field parameters for the heme prosthetic group of cytochrome c_i. *J. Comput. Chem.* **2004**, *25*, 1613−1622.

(55) Abraham, M. J.; Murtola, T.; Schulz, R.; Pall, S.; Smith, J. C.; Hess, B.; Lindahl, E. GROMACS: High Performance Molecular Simulations Through Multi-Level Parallelism from Laptops to Supercomputers. *SoftwareX* **2015**, *1−2*, 19−25.

(56) Darden, T.; York, D.; Pedersen, L. Particle mesh Ewald: An N·log(N) method for Ewald sums in large systems. *J. Chem. Phys.* **1993**, *98*, 10089−10092.

(57) Hunter, J. D. Matplotlib: A 2D graphics environment. *Comput. Sci. Eng.* **2007**, *9*, 90−95.

(58) Becke, A. D. Density Functional Thermochemistry. III. The Role of Exact Exchange. *J. Chem. Phys.* **1993**, *98*, 5648.

(59) Ditchfield, R.; Hehre, W.; Pople, J. A. Self-Consistent Molecular-Orbital Methods. IX. An Extended Gaussian-Type Basis for Molecular-Orbital Studies of Organic Molecules. *J. Chem. Phys.* **1971**, *54*, 724−728.

(60) Frisch, M. J.; Trucks, G. W.; Schlegel, H. B.; Scuseria, G. E.; Robb, M. A.; Cheeseman, J. R.; Scalmani, G.; Barone, V.; Mennucci, B.; Petersson, G. A.; Nakatsuji, H.; Caricato, M.; Li, X.; Hratchian, H. P.; Izmaylov, A. F.; Bloino, J.; Zheng, G.; Sonnenberg, J. L.; Hada, M.; Ehara, M.; Toyota, K.; Fukuda, R.; Hasegawa, J.; Ishida, M.; Nakajima, T.; Honda, Y.; Kitao, O.; Nakai, H.; Vreven, T.; Montgomery, J. A., Jr.; Peralta, P. E.; Ogliaro, F.; Bearpark, M.; Heyd, J. J.; Brothers, E.; Kudin, K. N.; Staroverov, V. N.; Kobayashi, R.; Normand, J.; Raghavachari, K.; Rendell, A.; Burant, J. C.; Iyengar, S. S.; Tomasi, J.; Cossi, M.; Rega, N.; Millam, N. J.; Klene, M.; Knox, J. E.; Cross, J. B.; Bakken, V.; Adamo, C.; Jaramillo, J.; Gomperts, R.; Stratmann, R. E.; Yazyev, O.; Austin, A. J.; Cammi, R.; Pomelli, C.; Ochterski, J. W.; Martin, R. L.; Morokuma, K.; Zakrzewski, V. G.; Voth, G. A.; Salvador, P.; Dannenberg, J. J.; Dapprich, S.; Daniels, A. D.; Farkas, Ö.; Ortiz, J. V.; Cioslowski, J.; Fox, D. J. *Gaussian 09*, revision A.1 ; Gaussian, Inc.: Wallingford, CT, 2009.

(61) Helgaker, T.; Jørgensen, P.; Olsen, J. *Molecular Electronic-Structure Theory*, 1st ed.; Wiley: New York, 2000.

(62) Sun, Q.; Berkelbach, T. C.; Blunt, N. S.; Booth, G. H.; Guo, S.; Li, Z.; Liu, J.; McClain, J. D.; Sayfutyarova, E. R.; Sharma, S.; Wouters, S.; Chan, G. K.-L. PySCF: The Python-based Simulations of Chemistry Framework. *Wiley Interdiscip. Rev.: Comput. Mol. Sci.* **2018**, *8*, No. e1340.

(63) Weigend, F.; Ahlrichs, R. Balanced Basis Sets of Split Valence, Triple Zeta Valence and Quadruple Zeta Valence Quality for H to Rn: Design and Assessment of Accuracy. *Phys. Chem. Chem. Phys.* **2005**, *7*, 3297−3305.

(64) Tomasi, J.; Persico, M. Molecular Interactions in Solution: An Overview of Methods Based on Continuous Distributions of the Solvent. *Chem. Rev.* **1994**, *94*, 2027−2094.

(65) Chai, J.-D.; Head-Gordon, M. Systematic Optimization of Long-Range Corrected Hybrid Density Functionals. *J. Chem. Phys.* **2008**, *128*, 084106.

(66) Skone, J. H.; Soudackov, A. V.; Hammes-Schiffer, S. Calculation of Vibronic Couplings for Phenoxyl/Phenol and Benzyl/Toluene Self-Exchange Reactions: Implications for Proton-Coupled Electron Transfer Mechanisms. *J. Am. Chem. Soc.* **2006**, *128*, 16655−16663.

(67) Van Voorhis, T.; Kowalczyk, T.; Kaduk, B.; Wang, L.-P.; Cheng, C.-L.; Wu, Q. The Diabatic Picture of Electron Transfer, Reaction Barriers, and Molecular Dynamics. *Annu. Rev. Phys. Chem.* **2010**, *61*, 149−170.

(68) Artiukhin, D. G.; Eschenbach, P.; Neugebauer, J. Computational Investigation of the Spin-Density Asymmetry in Photosynthetic Reaction Center Models from First Principles. *J. Phys. Chem. B* **2020**, *124*, 4873−4888.

(69) Webb, S. P.; Hammes-Schiffer, S. Fourier Grid Hamiltonian Multiconfigurational Self-Consistent-Field: A Method to Calculate Multidimensional Hydrogen Vibrational Wavefunctions. *J. Chem. Phys.* **2000**, *113*, 5214.

(70) Soudackov, A.; Hammes-Schiffer, S. *FGH_bspline revision 1.2.2009*; http://webpcet.chem.yale.edu (accessed Feb 4, 2021).

(71) Fain, B. *Theory of Rate Processes in Condensed Media*; Springer: Berlin Heidelberg, 1980.

(72) Cape, J. L.; Bowman, M. K.; Kramer, D. M. A Semiquinone Intermediate Generated at the Q_o Site of the Cytochrome bc_1 Complex: Importance for the Q-Cycle and Superoxide Production. *Proc. Natl. Acad. Sci. U. S. A.* **2007**, *104*, 7887−7892.

(73) Hoias Teixeira, M.; Menegon Arantes, G. Balanced Internal Hydration Discriminates Substrate Binding to Respiratory Complex I. *Biochim. Biophys. Acta, Bioenerg.* **2019**, *1860*, 541−548.

(74) Arantes, G. M. The Catalytic Acid in the Dephosphorylation of the Cdk2-pTpY/CycA Protein Complex by Cdc25B Phosphatase. *J. Phys. Chem. B* **2008**, *112*, 15244−15247.

(75) Kaila, V. R. I.; Hummer, G. Energetics of Direct and Water-Mediated Proton-Coupled Electron Transfer. *J. Am. Chem. Soc.* **2011**, *133*, 19040−19043.

(76) Klein, J. E. M. N.; Knizia, G. cPCET versus HAT: A Direct Theoretical Method for Distinguishing X-H Bond-Activation Mechanisms. *Angew. Chem., Int. Ed.* **2018**, *57*, 11913−11917.

(77) Politzer, P.; Harris, R. R. Properties of Atoms in Molecules. I. Proposed Definition of the Charge on an Atom in a Molecule. *J. Am. Chem. Soc.* **1970**, *92*, 6451−6454.

(78) Soudackov, A. V.; Hammes-Schiffer, S. Probing Non-adiabaticity in the Proton-Coupled Electron Transfer Reaction Catalyzed by Soybean Lipoxygenase. *J. Phys. Chem. Lett.* **2014**, *5*, 3274−3278.

(79) Harshan, A. K.; Yu, T.; Soudackov, A. V.; Hammes-Schiffer, S. Dependence of Vibronic Coupling on Molecular Geometry and Environment: Bridging Hydrogen Atom Transfer and Electron-Proton Transfer. *J. Am. Chem. Soc.* **2015**, *137*, 13545−13555.

(80) Cape, J. L.; Bowman, M. K.; Kramer, D. M. Reaction Intermediates of Quinol Oxidation in a Photoactivatable System that Mimics Electron Transfer in the Cytochrome bc_1 Complex. *J. Am. Chem. Soc.* **2005**, *127*, 4208−4215.

(81) Lundberg, M.; Siegbahn, P. E. M. Quantifying the Effects of the Self-Interaction Error in DFT: When do the Delocalized States Appear? *J. Chem. Phys.* **2005**, *122*, 224103.

(82) Bao, J. L.; Gagliardi, L.; Truhlar, D. G. Self-Interaction Error in Density Functional Theory: An Appraisal. *J. Phys. Chem. Lett.* **2018**, *9*, 2353−2358.

(83) Field, M. J.; Bash, P. A.; Karplus, M. A Combined Quantum Mechanical and Molecular Mechanical Poteintial for Molecular Dynamics Simulations. *J. Comput. Chem.* **1990**, *11*, 700−733.

(84) Arantes, G. M. Free Energy Profiles for Catalysis by Dual-Specificity Phosphatases. *Biochem. J.* **2006**, *399*, 343−350.

(85) Teixeira, M. H.; Curtolo, F.; Camilo, S. R. G.; Field, M. J.; Zheng, P.; Li, H.; Arantes, G. M. Modeling the Hydrolysis of Iron-Sulfur Clusters. *J. Chem. Inf. Model.* **2020**, *60*, 653−660.

Supporting Information

Tunneling and Nonadiabatic Effects on a Proton-Coupled Electron Transfer Model for the Q_o Site in Cytochrome bc_1

Sofia R. G. Camilo, Felipe Curtolo, Vanesa V. Galassi and Guilherme M. Arantes*

Department of Biochemistry, Instituto de Química, Universidade de São Paulo, Av. Prof. Lineu Prestes 748, 05508-900, São Paulo, SP, Brazil

Email: `garantes@iq.usp.br`

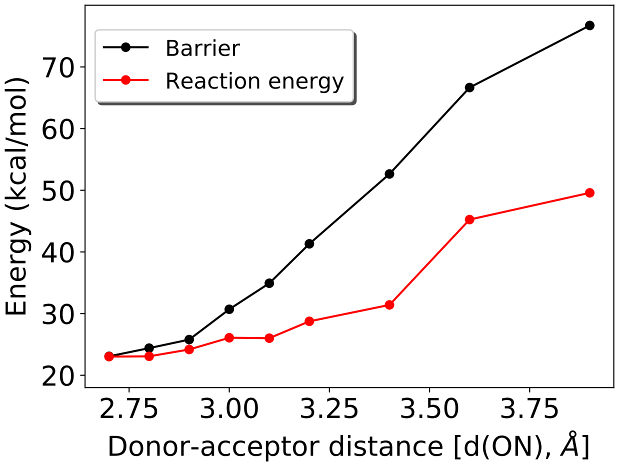

Figure S1: Reaction energy and barrier for the pure proton transfer reaction from quinol to imidazole (X=H in Fig. 2) for different donor-acceptor distance [d(ON)] obtained from B3LYP/6-31G* calculations. The reaction energies and barriers shown here were obtained by constrained geometry optimizations and may differ from the respective energies obtained by fully relaxed optimizations.

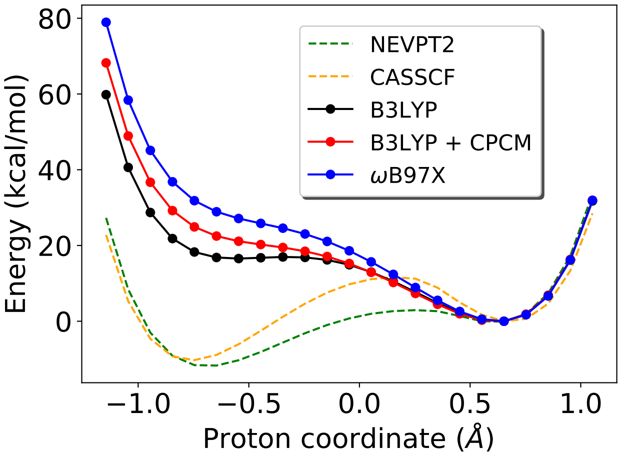

Figure S2: Comparison of adiabatic proton potentials for PCET from quinol to imidazole-iron(III)-sulfide, X=$[\text{Fe–S}]^{+1}$ in Fig. 2, in the TS orientation with distance d(ON)=2.7 Å. Potential energies were obtained for the same geometries and basis set (def2-SVP) with DFT functionals B3LYP (in vacuum and in the CPCM environment model) and ωB97X. Multiconfigurational CASSCF and NEVPT2 (same as green dashed curve in Fig. 5B) potentials were obtained from the corresponding diabatic energies with eq. 2 and shifted down so that the relative energy is zero in the PCET product ($PC = 0.60$ Å). Dynamic electron correlation, missing from the CASSCF curve and partially recovered by the NEVPT2 method, has a non-negligible contribution particularly near the avoided-crossing region. In comparison to the multiconfigurational surfaces, both DFT functionals destabilize the reactant basin (donor state) by 30-40 kcal/mol. Inclusion of a continuum model of the environment (CPCM) does not alter the shape of the potential significantly.

Table S1: Cartesian coordinates (Å) of planar orientation with d(ON)=2.7Å and PC=0.0 Å.

	x	y	z
S	2.84173243	-8.09430140	1.14492736
Fe	1.75627182	-6.39267394	0.74765468
N	0.57808594	-4.76043497	0.29060118
C	-0.71389130	-4.81239228	-0.22457247
C	0.89319268	-3.47143594	0.41051556
C	-1.15704720	-3.52682364	-0.40377689
N	-0.12824042	-2.69693608	0.00000000
C	-1.38903224	-6.11771312	-0.49463460
H	-2.39926341	-5.96281274	-0.88163368
H	-0.82514763	-6.70449513	-1.22837288
H	-1.45746356	-6.71663922	0.42013751
H	-2.09136083	-3.14304714	-0.78012511
H	1.83181195	-3.08673499	0.77976491
H	-0.01542763	-1.36041664	0.00000000
O	0.00000000	0.00000000	0.00000000
C	-0.64786395	1.02486847	-0.36426670
C	-1.84449898	0.91553664	-1.19427732
C	-2.60450705	2.02676583	-1.51164640
C	-2.16701562	3.29590120	-1.03787224
O	-2.88154359	4.39624477	-1.35033323
C	-1.00296625	3.45711236	-0.25954701
C	-0.20902840	2.36087703	0.05246934
O	0.89343903	2.59739894	0.78807256
C	2.00116774	1.67204993	0.83800335
C	-2.23200347	-0.46908658	-1.64231509
C	-3.86839105	1.94287664	-2.33522837
O	-0.68852122	4.75877849	0.07100073
C	-0.66149267	5.06650241	1.48284451
H	-1.34386551	-1.07661188	-1.83287872
H	-2.81919388	-0.97650377	-0.86586193
H	-2.83599040	-0.44881141	-2.55201104
H	-4.53207892	1.15908482	-1.95815986
H	-3.63991373	1.70684545	-3.38156805
H	-4.41260361	2.88753732	-2.32040767
H	-2.39932383	5.16066529	-0.98361027
H	-0.45031141	6.13474594	1.54789486
H	0.12331411	4.49642104	1.98380188
H	-1.63532598	4.84886417	1.93715982
H	2.82731049	2.25991030	1.24062435
H	1.77080014	0.82545036	1.48308051
H	2.24583553	1.31027655	-0.16402156

Table S2: Cartesian coordinates (Å) of TS orientation with d(ON)=2.7Å and PC=0.0 Å.

	x	y	z
S	-2.99269839	-7.58247297	-2.92947756
Fe	-2.60940524	-5.88315812	-1.80976120
N	-2.23080678	-4.22776013	-0.66489469
C	-2.73757333	-3.96822687	0.60257535
C	-1.45446214	-3.18470292	-0.98740503
C	-2.24567700	-2.75472894	1.01802707
N	-1.44631945	-2.27994110	0.00000000
C	-3.65065628	-4.92946233	1.29346102
H	-3.95036158	-4.54434612	2.27147371
H	-4.55583457	-5.10702726	0.70188589
H	-3.16231479	-5.89941750	1.44013060
H	-2.40049052	-2.20735930	1.93391284
H	-0.91357405	-3.07616504	-1.91519992
H	-0.69773044	-1.12896431	0.00000000
O	0.00000000	0.00000000	0.00000000
C	-0.01868141	0.83387713	0.94444382
C	-1.25175876	1.27205178	1.57350222
C	-1.22474670	2.21107520	2.59325475
C	0.02902507	2.73390243	2.99538745
O	0.07690499	3.64131258	3.98896546
C	1.25063403	2.33195183	2.39580970
C	1.24320827	1.40535569	1.38361391
O	2.40094258	1.13085466	0.75041763
C	2.76129435	-0.24728308	0.52332235
C	-2.55091118	0.71273750	1.05839480
C	-2.48417676	2.69428785	3.27211211
O	2.34519634	2.97344619	2.89456135
C	3.58275968	2.24751533	3.01973406
H	-2.43438227	0.32310049	0.04646012
H	-2.91599762	-0.10696507	1.69128703
H	-3.33383921	1.47562065	1.04409355
H	-3.12336137	1.85285570	3.55670993
H	-3.06844335	3.33445979	2.59966044
H	-2.25751554	3.27306777	4.16771012
H	1.01218970	3.88236294	4.12060813
H	4.14591326	2.76147024	3.80019281
H	4.12923353	2.26480973	2.07534436
H	3.39156569	1.21178281	3.31820391
H	3.85296398	-0.26409380	0.50128875
H	2.34903568	-0.59691517	-0.42374343
H	2.39643468	-0.88114771	1.33790107

Table S3: Cartesian coordinates (Å) of TS orientation with d(ON)=3.1Å and PC=0.0 Å.

	x	y	z
S	-6.48089025	-5.55791595	-3.10797196
Fe	-5.13119806	-4.46091502	-1.97110809
N	-2.32807552	-2.04695294	0.00000000
C	-2.83997463	-2.69998782	1.10051409
C	-3.80332781	-3.56799309	0.64379615
N	-3.87046575	-3.44370734	-0.73873180
C	-2.95768591	-2.51876631	-1.08103885
H	-2.76047303	-2.19151875	-2.09077306
C	-4.68425926	-4.51844496	1.38980788
H	-2.48522598	-2.50898529	2.10120268
H	-4.51793350	-5.55120856	1.06292315
H	-4.48956085	-4.46399650	2.46393902
H	-5.74314797	-4.29003743	1.22227205
H	-1.15877622	-1.04500546	0000000000
C	-0.12925614	1.29352344	3.40792653
C	1.26904668	1.31748356	3.65614421
C	2.21638271	0.98060652	2.66852943
C	1.79689684	0.62534591	1.39249486
C	0.37035000	0.48700360	1.13242884
C	-0.57105474	0.90410082	2.15095686
O	1.71705488	1.70374504	4.86961805
O	3.53532640	1.12074511	3.04060217
O	2.75731883	0.32261807	0.49598273
O	0.00000000	0.00000000	0.00000000
C	-2.03946781	0.90862039	1.80972492
H	2.69111690	1.70679356	4.82547758
H	-2.53539247	1.78894431	2.22876565
H	-2.19193039	0.91408255	0.72980358
H	-2.55658201	0.02803412	2.21109821
C	-1.08563394	1.70664654	4.49989456
H	-0.58240081	1.77406440	5.46484660
H	-1.52520423	2.68864835	4.28406385
H	-1.91226729	0.99493012	4.58874590
C	4.34446500	-0.07517154	2.99527026
C	2.54413496	0.47443922	-0.92420370
H	5.31448220	0.20880907	3.40569847
H	3.89385564	-0.86211821	3.61169785
H	4.45617328	-0.42291302	1.96650832
H	3.54713861	0.55917444	-1.34543399
H	2.02088707	-0.39076962	-1.33066384
H	1.96826360	1.37897797	-1.13474660